HHS Public Access

Author manuscript

Nanoscale. Author manuscript; available in PMC 2024 February 16.

Published in final edited form as:

Nanoscale. ; 15(7): 3273–3283. doi:10.1039/d3nr00248a.

Dextran/Eudragit S-100 based Redox Sensitive Nanoparticles for Colorectal Cancer Therapy

Aastha Gupta[a,#], **Ankita Dhiman**[a,#], **Ankur Sood**[a], **Ravi Bharadwaj**[b], **Neal Silverman**[b], **Garima Agrawal**[a,*]

[a]School of Chemical Sciences and Advanced Materials Research Centre, Indian Institute of Technology Mandi, H.P.- 175075, India

[b]Division of Infectious Diseases, Department of Medicine, University of Massachusetts Medical School, Worcester, Massachusetts, United States of America

Abstract

Herein, we present disulfide crosslinked dextran/eudragit S-100 nanoparticles (DEEU NPs) (≈ nm) for colorectal cancer treatment. These redox environment sensitive DEEU NPs are synthesized by simple oxidation of thiolated polymers in air. This approach allows avoiding the use of any additional chemical crosslinker. These DEEU NPs have high encapsulation efficiency for doxorubicin (DOX) model drug (≈95%). The prepared DEEU NPs are redox sensitive owing to disulfide units and exhibit ≈80% DOX release in reducing environment of GSH. Additionally, DOX-DEEU NPs display enhanced cytotoxicity for HCT116 cancer cells as compared to free DOX. Annexin V staining results also support the higher anticancer efficiency of DOX-DEEU NPs via induction of apoptosis. *In vivo* biodistribution results demonstrate that DEEU NPs can retain in the colon region up to 24 hours. These results indicate that DEEU NPs can act as a promising platform for colorectal cancer treatment.

Graphical Abstract

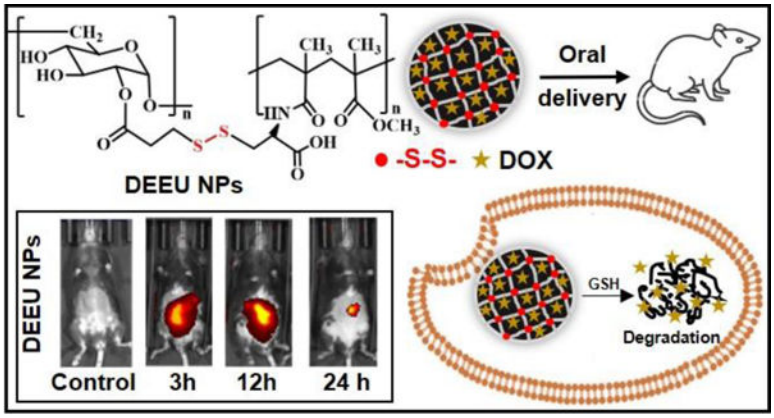

*Correspondence: garima@iitmandi.ac.in; Tel.: +91-1905267827.
#contributed equally to this work.

Conflict of Interests:
Authors declare no conflict of interests.

Synthesis of disulfide chemistry based redox sensitive DEEU NPs without using any additional chemical crosslinker for colorectal cancer.

Keywords

Dextran; Eudragit S-100; redox sensitive; nanoparticles; drug delivery; cancer

1. Introduction

Cancer is a prevalent disease worldwide, resulting in increasing mortality rate every year.[1–4] According to recent statistics, colorectal cancer is a common cancer in both the genders, and number of deaths caused by this cancer is expected to increase from 60% to 75% by 2035.[5, 6] To treat this disease, various drug delivery carriers such as nanoparticles, microgels, liposomes etc. have been developed so far.[7–12] However, their successful commercial application is still limited due to the lack of cytotoxic specificity, and the complex biological conditions of gastrointestinal tract.[13, 14]

Recently, extensive research has been done to utilize modern nanotechnology based concepts with various natural and synthetic polymers for developing a suitable drug delivery system.[15–17] Natural polymers display inherent biocompatibility and biodegradability making them a suitable candidate for preparing the carrier matrix.[18–20] On the other hand, synthetic polymers provide the possibility of having desired functional groups, and tuning the physicochemical properties by adjusting the synthetic strategy.[21–23] A combination of both natural and synthetic polymer offers the opportunity of developing the nanoparticle matrix in such a way that it can perform the desired action under complex biological environment. In this regard, dextran (DE) is a natural hydrophilic polymer showing enormous potential for biomedical applications.[18, 24–26] In case of synthetic polymers, eudragit S-100 (EU) is a hydrophobic copolymer having carboxylic groups.[13] It shows mucoadhesive properties, pH-dependent solubility behaviour, and resistance to gastric environment.[27–29] Based on the attractive properties of both DE and EU, they can be used in combination to synthesize nanoparticles that are efficient for oral administration for colorectal cancer.

A prime requirement during developing a nanoformulation for cancer therapy is its capability to degrade at the cancer site. Sufficient degradability of the nanoparticles helps in efficient drug release along with ensuring the removal of the degradation byproducts from the body. In this regard, various polymers responsive to different stimuli have been investigated.[2, 9, 30] Cancer cells exhibit ≈10 times higher amount of glutathione (GSH) as compared to normal healthy cells, which can be used as a trigger to degrade the nanoparticles once they enter the cancer cells. In this regard, disulfide crosslinked polymeric nanoparticles are of special interest as they can prevent the drug leakage under physiological conditions, and can effectively release the drug under reducing conditions caused by breaking of disulfide bonds.[13, 30, 31]

In this work, we synthesized homogeneous, biocompatible and biodegradable, redox stimulus sensitive dextran/eudragit S-100 nanoparticles (DEEU NPs) by simply reacting

thiolated dextran and thiolated eudragit S-100 in air atmosphere. This method enabled preparing the nanoparticles without using any additional chemical crosslinker. These DEEU NPs exhibited very high efficiency to encapsulate doxorubicin (DOX) anticancer drug. The reported nanoparticles system was colloidally stable under physiological environment, and released the drug upon treatment with GSH. Developed system was further investigated for *in vitro* and *in vivo* performance to analyse its applicability in colon cancer.

2. Materials and Methods

2.1. Materials

Dextran (DE) (Mw 40,000) was procured from Alfa Aesar, India. Eudragit S-100 (EU) was purchased from Evonik Industries, India. Fluorescein isothiocyanate (FITC), and doxorubicin (DOX, 98%) were procured from TCI Chemicals. L-cysteine (97%), mercaptopropionic acid (MPA, 99%), and glutathione reduced (GSH) were obtained from Sigma Aldrich, India. FITC-Annexin V Apoptosis Detection Kit was purchased from BD biosciences (559763).

2.2. Preparation of thiolated dextran (TDE)

Mercaptopropionic acid (MPA) was used for thiolation of dextran. Here, EDC and MPA were put together (2:1 molar ratio) in dimethyl formamide (5 mL) followed by stirring for 1 h. Afterward, dextran (50 mg/mL in water) was dropwise mixed into activated MPA solution (2.5:1 w/w). After overnight stirring, in the next step, the sample was precipitated in ethanol and further purified via centrifugation. Thus, obtained TDE (21 μg thiol/mg) was freeze dried and stored at 4 °C.

2.3. Preparation of thiolated eudragit S-100 (TEU)

Thiolation of eudragit S-100 was performed using L-cysteine by following the protocol as mentioned by Sood et al. with slight modification.[13] Briefly, EU, EDC, and NHS (10:1:1 w/w) were mixed and added to L-cysteine in water with EU: L-Cysteine ratio as 2:1 (w/w). Afterward, the sample was stirred for 3 h at pH 6. The obtained product was then precipitated using acetone followed by centrifugation. Obtained TEU (54 μg thiol/mg) was lyophilized and stored at 4 °C.

2.4. Fabrication of dextran/eudragit S-100 nanoparticles (DEEU NPs)

Four compositions of DEEU NPs were synthesized by varying the ratio of TDE and TEU (Table 1). To synthesize DEEU NPs, required quantity of TDE and TEU were mixed in water with subsequent stirring in air. Afterward, obtained nanoparticles were dialysed in water.

2.5. Determination of –SH content

DTNB assay was performed to measure the thiol content present in TDE, TEU and the different nanoformulations. Firstly, DTNB salt (0.03% (w/v)) was dissolved in PBS (pH 8). Next, 40 μL DTNB solution was mixed with 160 μL dispersion of TDE, TEU and

the different nanoformulations. After incubating the sample for 15 min, absorbance was obtained at 412 nm.

2.6. Degradation behaviour of DEEU NPs

DEEU NPs degradation in response to redox stimulus was analysed by investigating size variation of DEEU NPs in 10 mM GSH environment. Size was measured using dynamic light scattering at desired time points at 37 ºC. Additionally, scanning electron microscopy technique was also employed to determine DEEU NPs degradation in 10 mM GSH.

2.7. Drug loading in DEEU NPs (DOX-DEEU NPs) and *in vitro* drug release

As a general procedure, DOX (1 mg/mL) was dropwise added into 4.2 mg of DEEU NPs by maintaining the DOX:DEEU NPs as 1:10 (w/w). After overnight stirring at RT, purification was done via dialysis against water for 12 h. Aqueous medium from dialysis sink was further utilized to estimate the amount of free DOX (482 nm) via UV-Vis spectrophotometry. The loading efficiency and encapsulation efficiency were evaluated by using the following formula:

$$\%\ \ Encapsulation\ \ Effficiency\ \ (EE) = \frac{Amount\ \ of\ \ drug\ \ loaded}{Total\ \ drug\ \ added} X\ \ 100$$

$$\%\ \ Loading\ \ Efficiency\ \ (LE) = \frac{Amount\ \ of\ \ drug\ \ added}{Weight\ \ of\ \ nanoparticles} X\ \ 100$$

DOX release from DEEU NPs was performed in PBS having pH 7.4, and in 10 mM GSH. As a representative procedure, 4.2 mg DOX-DEEU NPs were kept in the dialysis bag and placed into a beaker containing 10 mM GSH (100 mL) under constant stirring. Afterward, 900 μL solution from sink was taken out at regular time intervals and same amount of fresh 10 mM GSH was added into it. The obtained solutions were analysed via UV-Vis spectrophotometry at 482 nm to estimate the cumulative release of DOX.

2.8. *In-vitro* cytotoxicity and cell proliferation

HCT116 cells (0.5×10^4 cells/well) were seeded overnight in 2% FBS containing DMEM media in a 96-well plate. Cells were treated with DEEU NPs, pure DOX drug, and DOX-DEEU NPs for 24 h at 37 °C and 5% CO_2. In the next step, 10 μL MTT solution per well was added and formazan crystals formed after 2 h were solubilized in 100 μL DMSO. Absorbance was noted at 570 nm and cell viability (%) was calculated as:

$$\%\ \ cell\ \ viability = \frac{absorbance\ \ of\ \ treated\ \ cells}{absorbance\ \ of\ \ control\ \ cells} * 100$$

To perform the cell proliferation study, HCT116 cells were seeded overnight at 0.5×10^4 cells/well density in 2% FBS-containing DMEM media. Afterward, the cells were treated with the IC50 value of DOX (2.3 μg/mL) DOX-DEEU NPs (35 μg/mL), and equivalent amount of pure DEEU NPs (35 μg/mL) for 24, 48, and 72 h after treatment. Cell proliferation was measured with MTT as mentioned above.

2.9. PE Annexin V-eFluor 450 staining

Annexin V staining was performed with HCT116 cells as per the manufacturer protocol (BD biosciences (559763). Briefly, HCT116 cells (0.5×10^6 cells/well) (in a 6-well plate) were seeded overnight in 2% FBS containing DMEM media. Cells were supplied with DOX (2.3 μg/L), DOX-DEEU NPs (35 μg/mL), and pure DEEU NPs (35 μg/mL) for 12 h at 37 °C. After harvesting and washing with PBS, cells were resuspended in 1× binding Buffer at a concentration of 1×10^5 cells/mL in 100 μL. Cells were stained by adding 5 μL PE Annexin V and 5 μL of LIVE/DEAD fixable aqua dead cell stain kit (Invitrogen) for 15 min at room temperature (RT). Samples were resuspended with 400 μl of 1X Binding Buffer to each tube and analysed with flow cytometry.

2.10. Cellular uptake of DEEU NPs

HCT116 or HEK293T cells were cultured in DMEM media supplied with 2% FBS with 5×10^4 cells density. Cells were incubated overnight and then supplied with FITC containing DEEU NPs (35 μg/mL) for 4 h. Cells were washed with warm PBS and fixed with 4% paraformaldehyde for 20 min at RT. Further, multiple washings with PBS were performed followed by mounting on a glass slide with DAPI containing mounting media (Thermo Fisher P36931).

2.11. *In vivo* biodistribution and *ex vivo* study

Indocyanine green (ICG)-tagged DEEU NPs were used to study the *in vivo* biodistribution of nanoparticles in 6−8 weeks old, female c57bl/6j mice. All animal studies were performed in compliance with the federal regulations set forth in the Animal Welfare Act (AWA), the recommendations in the Guide for the Care and Use of Laboratory Animals of the National Institutes of Health, and the guidelines of the UMass Chan Medical School Institutional Animal Use and Care Committee. All protocols used in this study were approved by the Institutional Animal Care and Use Committee at the UMass Chan Medical School with prior ethical clearance (protocol 202100174). Considering the mouse weight, ICG-tagged DEEU NPs were gavaged to three mice with 60 mg/kg dose. Separately, three mice with no DEEU NPs treatment were used as control. Biodistribution of ICG tagged DEEU NPs was followed at desired time points using the whole-body imager.

After 24 h of gavaging, mice were euthanized using CO_2 asphyxiation followed by cervical dislocation. Further, the mice were dissected to analyse the major organs like heart, liver, kidney, spleen, stomach, intestine and colon by whole body imager.

2.12. Characterization methods

The hydrodynamic diameter of different DEEU NPs formulations was analyzed using Malvern Zetasizer Nano ZS. It was done using a disposable cuvette and water as dispersing media.

Perkin Elmer model Spectrum Two (USA) FT-IR spectrometer was used to measure FT-IR spectra of various samples and the wavenumber range was set in between 500–4000 cm^{-1}. KBr pelleting method was used for the analysis where, a very little amount of KBr was

mixed uniformly with 1 mg of the desired sample, and a KBr pellet was created using a hydraulic press under 100 psi pressure for 30 seconds.

The morphology of DEEUNPs was analyzed using Nova Nano SEM-450 FESEM instrument. The sample was drop casted over a silicon wafer and sputtered with a gold coating to get a clear contrast.

Thermogravimetric analysis (TGA) was performed to check the thermal stability of various samples, using Netzsch-STA 449 Jupiter (Germany) model. The temperature range was selected from 25 °C to 900 °C in a nitrogen gas atmosphere with a heating rate of 10 °C/min.

Agilent Technologies, Cary Eclipse model was used to measure the pyrene probe-based fluorescence. Briefly, 50 μg of the desired sample was dispersed into 3 mL acetone and the spectra were recorded from 360 nm to 450 nm at room temperature to check the intensity of peaks.

Confocal Laser Scanning Microscopy (CLSM) (Leica, SP8) was used for cellular uptake study. Cells were tagged with FITC and placed on glass slide using DAPI based mounting media. Samples were analysed using Cytec aurora flow cytometer.

In vivo and *ex vivo* biodistribution study were performed using a PerkinElmer IVIS whole body imager where ICG was used as a fluorescent probe. For this study, considering the mouse weight, ICG-tagged DEEU NPs were orally gavaged to three mice with 60 mg/kg dose.

2.13. Statistical data analysis

Statistical analysis was done by Analysis of Variance (ANOVA) with $p < 0.05$.

3. Results and Discussion

3.1. Preparation and characterization of DEEU NPs

Synthesis of DEEU NPs was performed based on the idea of simply crosslinking thiolated dextran (TDE) and thiolated eudragit S-100 (TEU) in air atmosphere using disulfide chemistry (Figure 1). To synthesize TDE, –OH groups present in dextran were reacted with –COOH functionality present in MPA. In a separate step, to prepare TEU, –COOH functionality of EU was employed for chemical modification by $–NH_2$ groups of L-cysteine.

Based on Elman's reagent test, amount of free −SH in TDE and TEU was calculated as 21 and 54 μg thiol/mg NPs. Considering the thiol content of both the thiolated polymers, four different DEEU NPs formulations were developed varying the ratio of TDE and TEU in the range of 1:0.25 to 1:1 (Table 1). All the nanoparticulate formulations were then characterized via dynamic light scattering to analyse the size and size distribution. Based on the experimental results, it is clear that DEEU-2 NPs had the smallest size (235 nm), lowest polydispersity index (PDI) (0.16), and minimum free thiol content 0.49 μg thiol/mg NPs as compared to the other samples (Table 1). A detailed analysis of different runs of each sample along with the error bars for hydrodynamic dimeter (D_{Hyd}), and PDI is presented as Table

S1 in the supplementary information. Based on these results, DEEU−2 NPs was chosen for further study and to investigate its applicability for efficient drug delivery in cancer therapy. It is to be noted that from this point onward, DEEU−2 NPs has been denoted as DEEU NPs for further discussion.

To investigate the morphology and size distribution of DEEU NPs, SEM measurement was performed. Figure 2A displays SEM image of DEEU NPs showing that the prepared nanoparticles were homogeneous and spherical in morphology. Size distribution histogram presented in figure 2B exhibits that the average size of the developed DEEU NPs was approximated to 55 nm. The variation in size obtained from SEM as compared to DLS can be attributed to the SEM operating conditions where the measurement was done in the dried state. Also, in case of DLS, the recorded size is the hydrodynamic diameter of the nanoparticles which includes not only the diameter of the nanoparticles but also the solvent layer around it. This results in the difference of size obtained from DLS and SEM for DEEU NPs.

Figure 3 presents the comparative FTIR analysis of DE, TDE, EU, TEU, and DEEU NPs to gain deeper insight into the chemical functionalities present in polymer structure. Figure 3A exhibits the comparison of pure DE and TDE. Here, −OH and C−H stretching of dextran were observed at 3434 cm^{-1} and 2929 cm^{-1} respectively. Further, peaks corresponding to C−O−C and C−O stretching vibrations were obtained at 1152 cm^{-1} and 1104 cm^{-1} respectively. In case of TDE, apart from the characteristic peaks of dextran, −C=O stretching of ester bond was observed at 1660 cm^{-1} while S−H stretching peak was obtained at 2561 cm^{-1}. The absence of these peaks in pure DE confirms the successful thiolation of dextran resulting in TDE formation. Further, a comparison of EU and TEU was made in Figure 3B. In case of EU, peaks corresponding to −C−H stretching, carboxylic −C=O stretching, methyl −C−H bending, and −C−O stretching were obtained at 2950, 1725, 1448, and 1161 cm^{-1} respectively. In case of TEU, additional peaks corresponding to S−H stretching, amide C=O stretching, and amide N−H bending were observed at 2578 cm^{-1}, 1637 cm^{-1}, and 1558 cm^{-1} confirming the successful thiolation. It is clear from Figure 3C that the thiol peaks from TDE and TEU were absent in case of DEEU NPs confirming the crosslinking via disulfide-based chemistry.

To investigate the presence of both hydrophilic and hydrophobic regions in DEEU NPs, fluorescence of pyrene was analysed in different chemical environment. Based on the fluorescence spectra of pyrene in TDE, DEEU NPs, and TEU, I_{392}/I_{372} ratio was obtained as 0.80 (in TDE), 0.82 (in DEEU NPs), 0.84 (in TEU), and 0.79 (pure pyrene) respectively. The increase in the value of I_{392}/I_{372} indicates the existence of hydrophobic regions in DEEU NPs which can be attributed to the presence of eudragit S-100 in the developed nanoparticles. Comparative fluorescence spectra are presented in Figure S1.

Further, thermogravimetric analysis was done to investigate the degradation behaviour of DE, EU, and DEEU NPs in response to the increase in the temperature (Figure 4). In case of DE, initial weight loss (8 wt%) between 40 to 170 °C was ascribed to the release of the moisture. Next, sharp degradation was observed between 260 to 390 °C which is a characteristic degradation behaviour of dextran leading to 80% weight loss. Finally, between

400 to 570 °C further degradation occurred showing 10.9% weight loss resulting in residual remains of 1%. Similar results have also been mentioned elsewhere.[32, 33] On the other hand, TGA analysis of EU displayed degradation in three steps. In the first step, 5% weight loss was seen between 50 °C to 180 °C due to moisture removal from polymer. Further, 85.4% weight loss was observed in the second step between 170 °C to 450 °C, followed by 8% weight loss between 450 °C to 510 °C in the third step due to the degradation of the polymer backbone resulting in 1.5% residual weight. It was observed that DEEU NPs formed via disulfide chemistry exhibited the degradation behaviour of both DE and EU with 0.12% residual weight.

To study the stability of DEEU NPs, the variation in size of DEEU NPs was followed by DLS over 48 h in 0.1M PBS, pH 7.4 at 37 ºC for the desired time intervals (Figure 5A). It was observed that DEEU NPs exhibited excellent colloidal stability. Representative size distribution curves, obtained at the initial time point and after 48 h, have been shown in Figure S2 for comparison. To further analyse the stability related to surface charge of DEEU NPs, zeta potential measurements were done. It is to be noted that zeta potential values for DEEU NPs in water at 0 h and 48 h were −24.6 mV and −24.7 mV respectively. These results are in correlation with the stability results obtained from DLS. On the other hand, zeta potential values in PBS at 0 h was −11.9 mV and at 48 h was −10.6 mV. Significantly negative zeta potential values in PBS shows that DEEU NPs are stable even in the presence of salts.

One of the crucial parameters while designing a drug delivery carrier is the sufficient degradability of the carrier in response to the desired stimuli. This is required to avoid bioaccumulation of the degraded by-products along with facilitating the drug release at the target site. To investigate the degradation behaviour, DLS measurement were done to track the changes in hydrodynamic size of DEEU NPs upon treatment with 10 mM GSH over 48 h. It is clear from the results displayed in Figure 5B that DEEU NPs initially showed swelling upon treating the sample with 10 mM GSH. This is attributed to the partial degradation of existing disulfide bonds leading to lesser crosslinking. With increasing time, breaking of disulfide bonds increased resulting into the degradation of DEEU NPs. Furthermore, the degradation of DEEU NPs was also followed by SEM. Figure 5C presents the SEM image of DEEU NPs after 48 h at pH 7.4. It is clear from the image that DEEU NPs were stable under these conditions. On the other hand, figure 5D clearly shows the degradation of DEEU NPs after 48 h under 10 mM GSH conditions.

3.2. In vitro release of DOX

DOX was used as a model drug to investigate the *in vitro* drug release pattern of the developed DEEU NPs to check their suitability for drug delivery application. DEEU NPs exhibited 8.6% loading efficiency and 95% encapsulation efficiency for DOX (Figure 6). To estimate the drug release under normal physiological conditions, experiments were performed in PBS at pH 7.4. Here, ~30% DOX was released after 3 h, while ~34% release was observed after 48 h. On the other hand, to estimate the drug release under the conditions of cancer cells, DOX release was performed under reducing environment of 10 mM GSH. GSH environment helped in the breaking of disulfide bonds resulting in ≈60% DOX release

after 3 h. Overall, approximately 80% DOX release was observed after 48 h due to the degradation of the particles in GSH. These results indicate that DEEU NPs can be utilized for cancer treatment.

3.3. In vitro cytotoxicity and cell proliferation analysis

Cytotoxicity behaviour for different concentrations of DOX, DEEU NPs, and DOX-DEEU NPs against HCT116 cells was analysed using MTT assay (Figure 7A). The experimental results exhibited that DOX, and DOX-DEEU NPs reduced the percent cell viability of HCT116 cells in a dose dependent manner. IC50 value of DOX was around 2.3 μg/mL. In case of DOX loaded DEEU NPs, IC50 was 2.2 μg/mL w.r.t to DOX which is an equivalent of around 35 μg/mL DOX-DEEU NPs. On the other hand, DEEU NPs were nontoxic with >90% cell viability at all respective doses in the concentration range of 1–100 μg/mL confirming their biocompatibility. The cell viability % was highest for DEEU NPs followed by free DOX, while DOX-DEEU NPs exhibited the lowest cell viability %. The obtained results indicate the efficiency of DOX-DEEU NPs for killing colon cancer cells as compared to pure DOX drug.

Further, the cell proliferation activity of DEEU NPs, DOX, and DOX-DEEU NPs was analyzed in a time dependent manner (Figure 7B). It was observed that the cytotoxic effect of DEEU NPs was insignificant for 24 h, however, it showed some significance over 48 and 72 h. Here, cell proliferation was almost similar for both 48 and 72 h post treatment with DEEU NPs. As the cell proliferation assay is performed without removal of the initial media, it is speculated that due to the time dependent accumulation of nanoparticles inside the cells the total surface area of interaction of DEEU NPs increases, resulting in more chances for their interactions with surrounding biomolecules. It is hypothesized that it could have resulted in the activation of urea and albumin synthetic pathways which in turn results in some toxic effect in the cells. This could have resulted in the observed toxic effects of DEEU NPs upon incubation for 48 and 72 h. Similar results have been reported by Gokduman et al.[34] In case of DOX treated group, the cell proliferation was significantly restricted and showed time dependent decrement in cell proliferation. Similar trend was observed in case of DOX-DEEU NPs exhibiting continuous decrease in cell proliferation in the DOX-DEEU NPs treated group. Although minimal difference is observed in the level of decrease in the cell proliferation between free DOX and DOX-DEEU NPs, yet it is to be noted that this difference is in the *in vitro* setups at the laboratory scale, and this distinction will be substantial upon clinical translations. These results demonstrated that DOX-DEEU NPs have more pronounced effect in inhibiting the proliferation of HCT116 cancer cells compared to DOX alone.

3.4. Cell death analysis by PE Annexin V-eFluor 450 staining

Flow cytometry analysis of HCT116 cells is shown in Figure 8. Here PE Annexin V was used which is a sensitive probe to identify apoptotic cells, as it binds with negatively charged phospholipid membranes with a very high affinity for phosphatidylserine (PS). As observed in Figure 8, there was a single cell population in case of control (Figure 8A) and DEEU NPs (Figure 8B) indicating viable cells. In case of DOX treated group (Figure 8C), two different sets of population were observed with less viable cells. This observation looks more evident

in case of the group treated with DOX-DEEU NPs (Figure 8D). A comparative analysis of the pre-apoptotic cell population is indicated in Figure 8I, where the numbers were substantially high for DOX and DOX-DEEU NPs treated groups. This is an indication of the targeting efficiency and adequate internalization of DOX-DEEU NPs against HCT 116 cells. Further, the efluor450 dye was used to assess the membrane integrity where they get bound to apoptotic cells (higher level) and to viable cells (low level). Typical dead cell population was recorded using efluor 450 and the results are shown in Figure 8E-H for control, DEEU NPs, DOX, and DOX-DEEU NPs respectively. It was further observed that high dead cell population was related to DOX and DOX-DEEU NPs as compared to control and DEEU NPs treated groups where the dead cell population was marginally higher (Figure 8I-J). The analysis further supports the targeting efficiency and uniform distribution of DOX-DEEU NPs inside the cells.

3.5. Cellular uptake

In order to determine the *in vitro* targeting efficiency of DEEU NPs toward colorectal cancer cells as compared to normal cells, cellular uptake analysis of DEEU NPs was performed using CLSM. Figure 9 is a set of confocal images depicting cellular uptake of DEEU NPs in HCT116 cells (colorectal cancer cells) (Figure 9A) and HEK293T cell line (normal cell line) (Figure 9B). It was observed that the nuclei were pronounced in both the cases with clear fluorescent signals that were detected in blue channel, while FITC tagged DEEU NPs appeared to be internalized more in case of HCT116 cells than HEK293T cells. Also, the rate of internalization of DEEU NPs in case of HCT116 cells increased in a time dependent manner. Here, the fluorescent signals in the green channel were less evident for the first 15 min followed by gradual increment leading to intense signals appearing at 4 h. Further, the specificity of DEEU NPs towards colorectal cells was also supported by the uniform distribution of DEEU NPs inside the colorectal cells. It is in correlation with the previous reports which suggest the targeting efficiency of Eudragit S-100 and dextran for colon sites.[35–37] It is also speculated that the presence of dextranases (responsible for degrading the dextran chains) at the colon site could also be a vital rationale for the specificity of DEEU NPs towards colon cells.[35]

Further, it is to be noted that free DOX drug is not only internalized by HCT116 cancer cells but also by normal HEK293T cells indicating the harmful effects of free drugs on healthy cells (Supporting information, Figure S3). These results clearly show that the use of DOX-DEEU NPs can help reducing the adverse effects on healthy cells in comparison to pure free DOX drug. Cellular uptake of pure DEEU NPs in HCT116 cancer cells has been presented in Supporting information, Figure S4.

3.6. *In vivo* and *ex vivo* biodistribution

The targeting efficiency and *in vivo* biodistribution of the designed DEEU NPs were evaluated using a non-invasive NIR fluorescence imaging technique. The *in vivo* biodistribution of DEEU NPs is presented in Figure 10A. It was observed that 1 h post-administration, the DEEU NPs were localized to the liver, kidney, and spleen. After 6 h, high-intensity signals appeared in the kidney and liver region with the onset of DEEU NPs movement towards the stomach region. Higher uptake of DEEU NPs in the liver

and spleen region could be accounted for the mononuclear phagocytic system associated with these organs. This associated phagocytic system acts as the prime barrier for tumor targeting through nanoparticles. Further, the clearance from liver and continued movement towards the stomach region was seen till 12 h post-administration. At the end of 24 h, negligible signals were recorded even from the stomach region which could be ascribed to the clearance of the majority of DEEU NPs from the stomach region.

Further, the retention of DEEU NPs, 24 h post-oral administration in different organs was recorded *ex vivo* (Figure 10B). In the case of *ex vivo* distribution, the highest fluorescence signals were recorded from the colon and stomach area while nominal or no signals were obtained from other major organs. The *ex vivo* distribution indicated the colon-targeting ability of the designed DEEU NPs. Also, as signals in the stomach region are decreased by 24 h post-administration, it is speculated that further time increments in the endpoint for *ex vivo* distribution could result in complete colon localization of the designed DEEU NPs.

Conclusion

In this work, redox stimulus sensitive DEEU NPs were synthesized by thiol chemistry-based crosslinking of TDE and TEU in the presence of air. Here, this approach allowed to avoid the use of any additional chemical crosslinker for preparing the nanoformulation. DEEU NPs had high efficiency to encapsulate DOX (≈95%) which was used as a model anticancer drug in this work. The developed DEEU NPs were able to control the undesired release of DOX under physiological conditions. On the other hand, taking the advantage of disulfide bonds, ≈80% DOX was released under 10 mM GSH conditions representing the cancer environment. The reported DEEU NPs were nontoxic up to 100 μg/mL, while DOX-DEEU NPs had higher efficiency for killing HCT116 colon cancer cells as compared to free DOX. *In vivo* and *ex vivo* biodistribution studies further confirmed the ability of DEEU NPs to target colon cancer, thus presenting them as a promising platform for colorectal cancer therapy.

Supplementary Material

Refer to Web version on PubMed Central for supplementary material.

Acknowledgement

Support from Department of Science & Technology, India (No. INT/Korea/P-60) (GA) and NIH United States (RO1 AI060025) (NS) are highly acknowledged. Authors thank AMRC, IIT Mandi for infrastructure support.

Abbreviations:

DE	Dextran
EU	Eudragit S-100
GSH	Glutathione
DEEU NPs	Dextran/Eudragit S-100 nanoparticles

DOX	Doxorubicin
FITC	Fluorescein isothiocyanate
MPA	Mercaptopropionic acid
EDC	[1-Ethyl-3-(3-dimethylaminopropyl)-carbodiimide]
NHS	N-Hydroxysuccinimide
TDE	Thiolated dextran
TEU	Thiolated eudragit S-100
DTNB	5,5′-dithiobis-(2-nitrobenzoic acid)
ICG	Indocyanine green
FESEM	Field emission scanning electron microscopy
CLSM	Confocal Laser Scanning Microscopy
FTIR	Fourier-transform infrared spectroscopy
PDI	Polydispersity index
MTT	3-(4,5-dimethylthiazol-2-yl)-2,5-diphenyltetrazolium bromide
FBS	Fetal Bovine Serum
DMEM	Dulbecco’s Modified Eagle Medium
HEK293	Human embryonic kidney cells
HCT116	Human colorectal carcinoma cell

References

1. Schmitt M and Greten FR, Nature Reviews Immunology, 2021, 21, 653–667.
2. Agrawal G, Agrawal R and Pich A, Particle & Particle Systems Characterization, 2017, 34, 1700132.
3. Soerjomataram I and Bray F, Nature reviews Clinical oncology, 2021, 18, 663–672.
4. Xi Y and Xu P, Translational Oncology, 2021, 14, 101174. [PubMed: 34243011]
5. Douaiher J, Ravipati A, Grams B, Chowdhury S, Alatise O and Are C, Journal of Surgical Oncology, 2017, 115, 619–630. [PubMed: 28194798]
6. Sawicki T, Ruszkowska M, Danielewicz A, Niedźwiedzka E, Arłukowicz T and Przybyłowicz KE, Cancers, 2021, 13, 2025. [PubMed: 33922197]
7. Agrawal G and Agrawal R, Small, 2018, 14, 1801724.
8. Agrawal G and Agrawal R, Polymers, 2018, 10, 418. [PubMed: 30966453]
9. Agrawal G, Samal SK, Sethi SK, Manik G and Agrawal R, Polymer, 2019, 178, 121599.
10. Handali S, Moghimipour E, Rezaei M, Ramezani Z, Kouchak M, Amini M, Angali KA, Saremy S and Dorkoosh FA, Biomedicine & Pharmacotherapy, 2018, 108, 1259–1273. [PubMed: 30372827]
11. Xie P, Wang Y, Wei D, Zhang L, Zhang B, Xiao H, Song H and Mao X, Journal of Materials Chemistry B, 2021, 9, 5173–5194. [PubMed: 34116565]

12. Gavas S, Quazi S and Karpiński TM, Nanoscale Research Letters, 2021, 16, 1–21. [PubMed: 33387075]
13. Sood A, Gupta A, Bharadwaj R, Ranganath P, Silverman N and Agrawal G, Carbohydrate Polymers, 2022, 294, 119833. [PubMed: 35868778]
14. Rychahou P, Bae Y, Reichel D, Zaytseva YY, Lee EY, Napier D, Weiss HL, Roller N, Frohman H and Le A-T, Journal of controlled release, 2018, 275, 85–91. [PubMed: 29421609]
15. Gupta A, Sood A, Fuhrer E, Djanashvili K and Agrawal G, ACS Biomaterials Science & Engineering, 2022, 8, 2281–2306. [PubMed: 35513349]
16. Sood A, Arora V, Kumari S, Sarkar A, Kumaran SS, Chaturvedi S, Jain TK and Agrawal G, International Journal of Biological Macromolecules, 2021, 189, 443–454. [PubMed: 34425122]
17. Wong KE, Ngai SC, Chan K-G, Lee L-H, Goh B-H and Chuah L-H, Frontiers in pharmacology, 2019, 10, 152. [PubMed: 30890933]
18. Sood A, Gupta A and Agrawal G, Carbohydrate Polymer Technologies and Applications, 2021, 2, 100067.
19. Zheng Y, Xie Q, Wang H, Hu Y, Ren B and Li X, International Journal of Biological Macromolecules, 2020, 165, 2668–2683. [PubMed: 33115646]
20. Liu Z, Jiao Y, Wang Y, Zhou C and Zhang Z, Advanced drug delivery reviews, 2008, 60, 1650–1662. [PubMed: 18848591]
21. Agrawal G, Wang J, Brüster B, Zhu X, Möller M and Pich A, Soft Matter, 2013, 9, 5380–5390.
22. Agrawal G, Schürings MP, van Rijn P and Pich A, Journal of Materials Chemistry A, 2013, 1, 13244–13251.
23. Wiemer K, Dörmbach K, Slabu I, Agrawal G, Schrader F, Caumanns T, Bourone SDM, Mayer J, Steitz J, Simon U and Pich A, Journal of Materials Chemistry B, 2017, 5, 1284–1292. [PubMed: 32263596]
24. Hu Q, Lu Y and Luo Y, Carbohydrate polymers, 2021, 264, 117999. [PubMed: 33910733]
25. Huang G and Huang H, Nanomedicine, 2018, 13, 3149–3158. [PubMed: 30516091]
26. Tekie FSM, Soleimani M, Zakerian A, Dinarvand M, Amini M, Dinarvand R, Arefian E and Atyabi F, Carbohydrate polymers, 2018, 201, 131–140. [PubMed: 30241804]
27. Kumar VS, Rijo J and Sabitha M, International journal of biological macromolecules, 2018, 110, 318–327. [PubMed: 29378277]
28. Thakral NK, Ray AR and Majumdar DK, Journal of Materials Science: Materials in Medicine, 2010, 21, 2691–2699. [PubMed: 20535630]
29. Bansal D, Gulbake A, Tiwari J and Jain SK, International journal of biological macromolecules, 2016, 82, 687–695. [PubMed: 26464131]
30. Sauraj, Vinay k., Kumar B, Priyadarshi R, Deeba F, Kulshreshtha A, Kumar A, Agrawal G, Gopinath P and Negi YS, Materials Science and Engineering: C, 2020, 107, 110356. [PubMed: 31761247]
31. Iyer R, Nguyen T, Padanilam D, Xu C, Saha D, Nguyen KT and Hong Y, Journal of Controlled Release, 2020, 321, 363–371. [PubMed: 32061622]
32. Kanakia S, Toussaint JD, Chowdhury SM, Lalwani G, Tembulkar T, Button T, Shroyer KR, Moore W and Sitharaman B, International journal of nanomedicine, 2013, 8, 2821. [PubMed: 23946653]
33. Yin R, Han J, Zhang J and Nie J, Colloids and Surfaces B: Biointerfaces, 2010, 76, 483–488. [PubMed: 20074919]
34. Gokduman K, Bestepe F, Li L, Yarmush ML and Usta OB, Nanomedicine, 2018, 13, 1267–1284. [PubMed: 29949471]
35. Hovgaard L and Brøndsted H, Journal of Controlled Release, 1995, 36, 159–166.
36. Shrivastava P, Singh R and Shrivastava S, Chemical Papers, 2010, 64, 592–601.
37. Shrivastava PK and Shrivastava SK, Current Drug Delivery, 2010, 7, 144–151. [PubMed: 20158488]

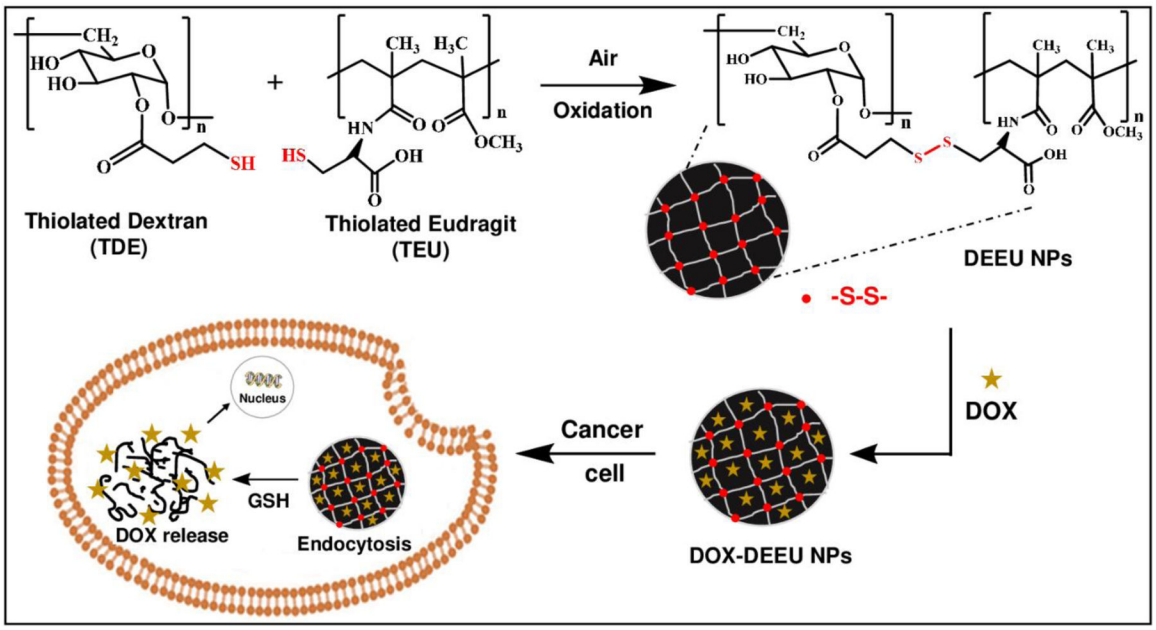

Figure 1.

Scheme showing synthesis of DEEU NPs using thiolated dextran and thiolated eudragit S-100 via air oxidation, loading of DEEU NPs with DOX, and drug release in response to redox stimulus in cancer cells.

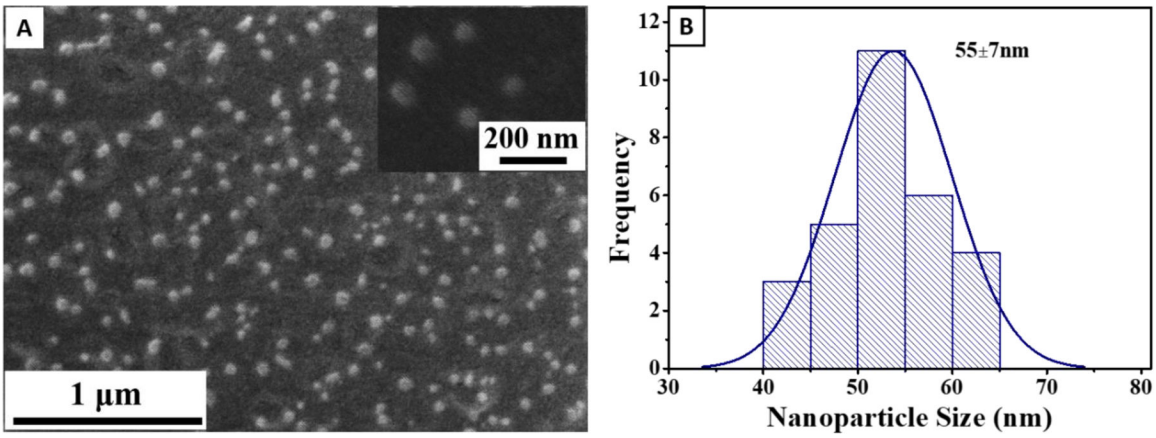

Figure 2.
Scanning electron microscopy image of DEEU NPs (A); size distribution histogram of DEEU NPs (B).

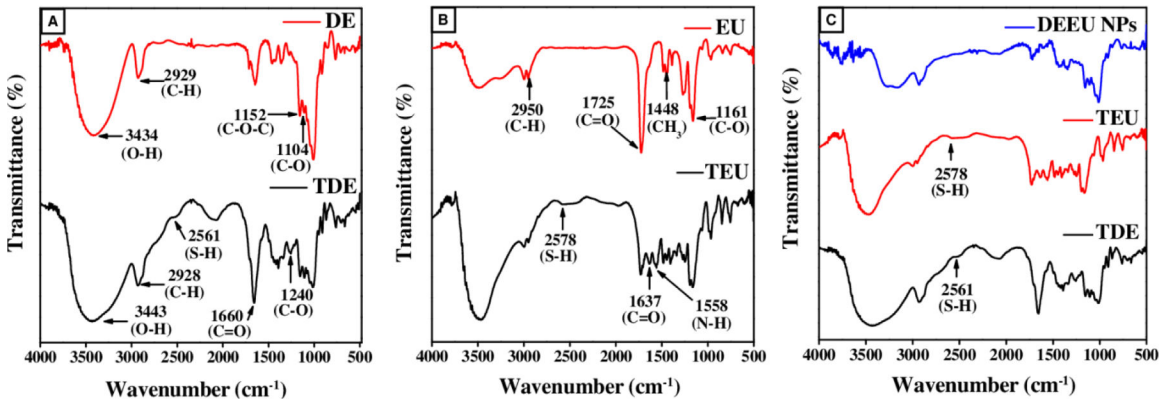

Figure 3.

Comparative FTIR spectra of dextran (DE) and thiolated dextran (TDE) (A); eudragit S-100 (EU) and thiolated eudragit S-100 (TEU) (B); TDE, TEU, and DEEU NPs (C).

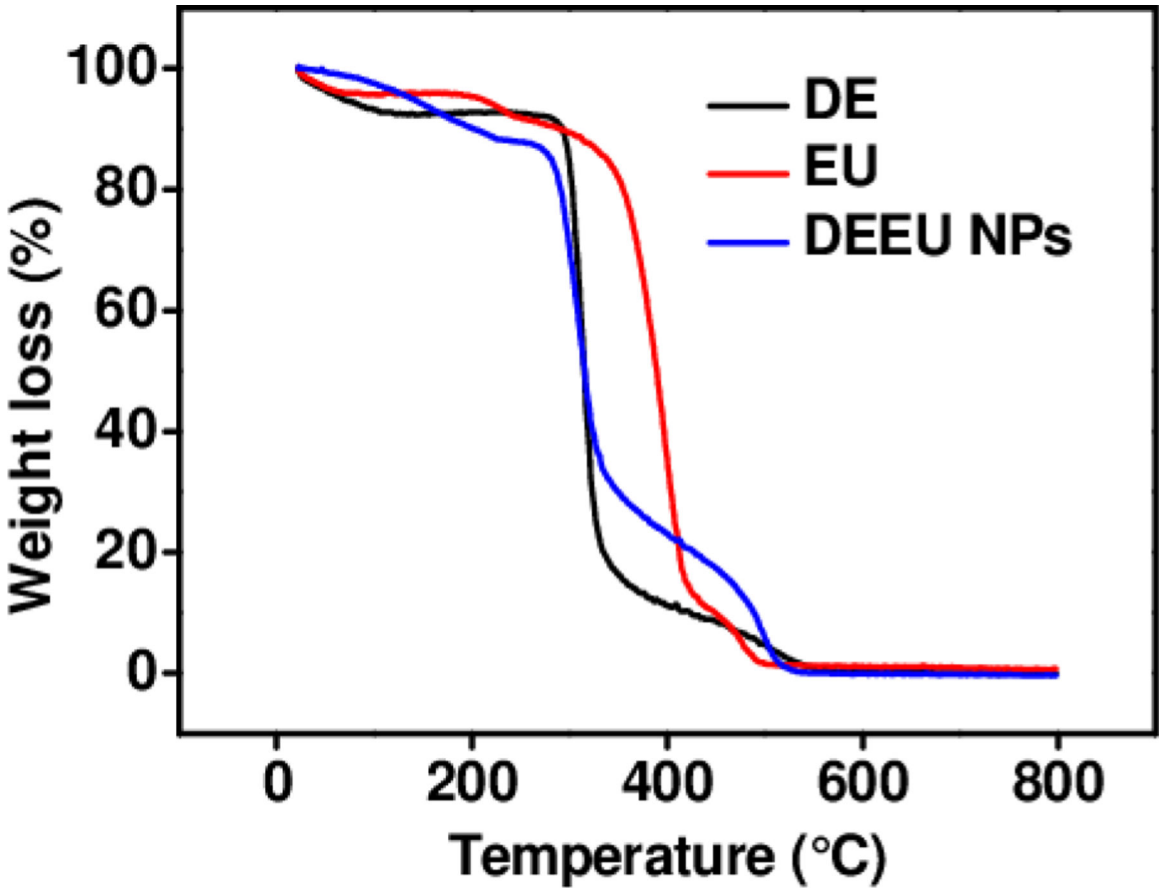

Figure 4.
Comparative thermogravimetric analysis of DE, EU, and DEEU NPs.

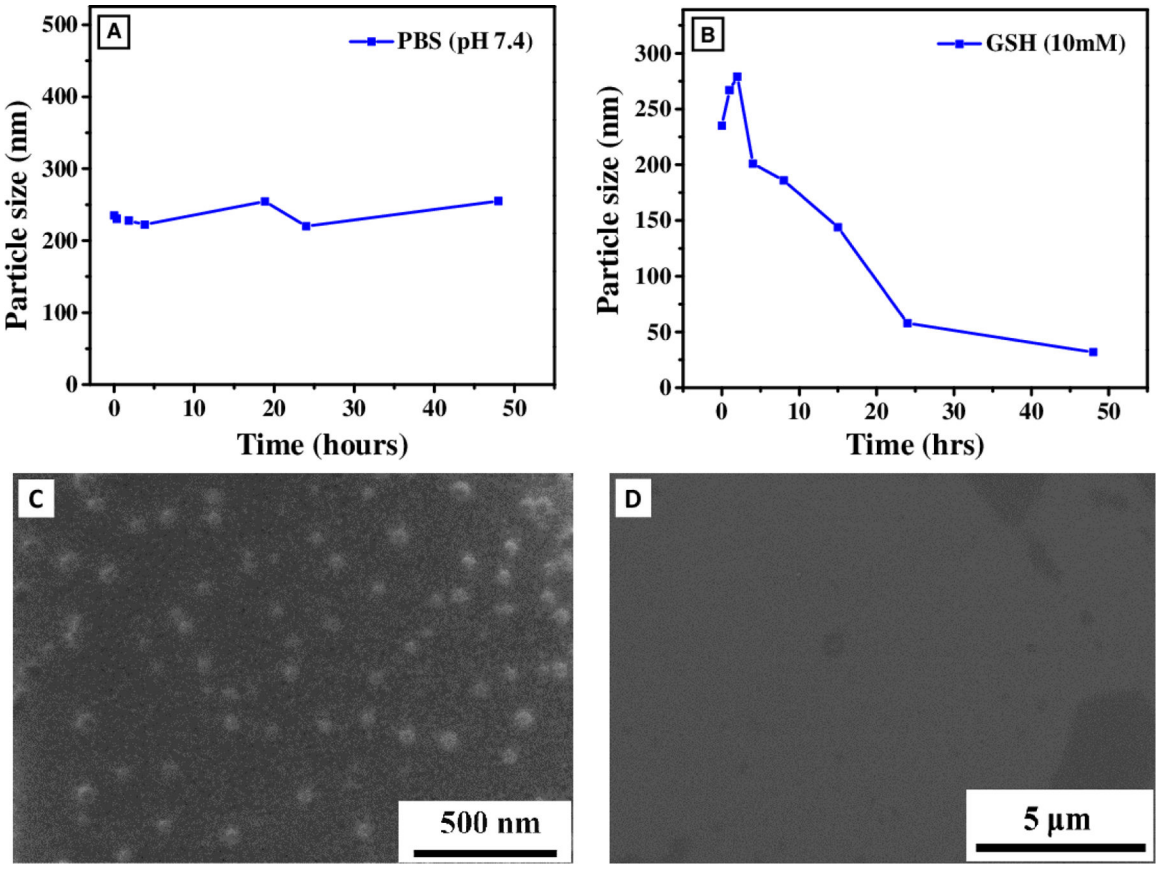

Figure 5.

Hydrodynamic size of DEEU NPs in PBS, pH 7.4 at 37 ºC at regular time intervals up to 48 h (A); variation in the hydrodynamic size of DEEU NPs in the presence of 10 mM GSH at regular time intervals indicating the nanoparticle degradation (B); FESEM image of DEEU NPs in PBS, pH 7.4 after 48 h (C); FESEM image of DEEU NPs in 10 mM GSH after 48 h (D).

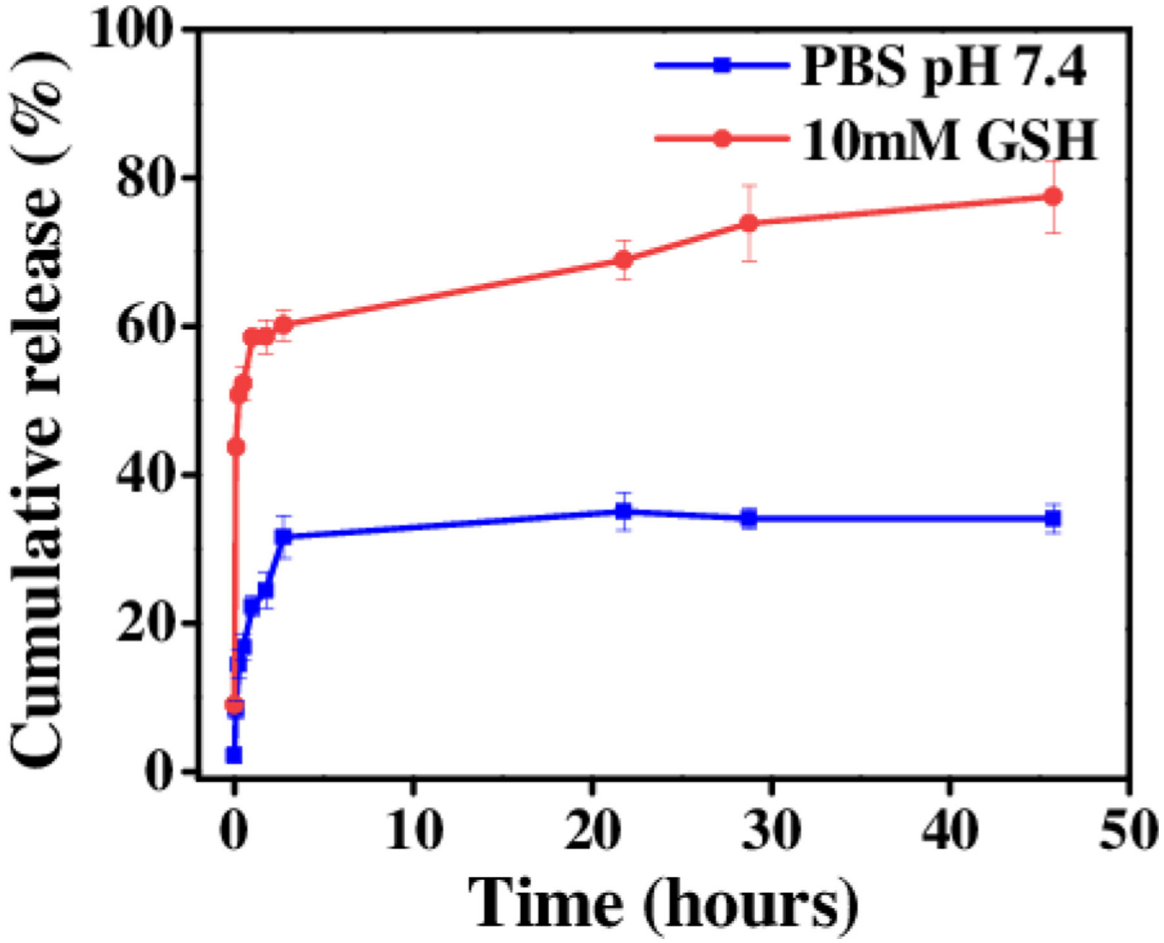

Figure 6.
In vitro release of DOX from DOX-DEEU NPs at PBS (pH 7.4), and 10 mM GSH as a function of time.

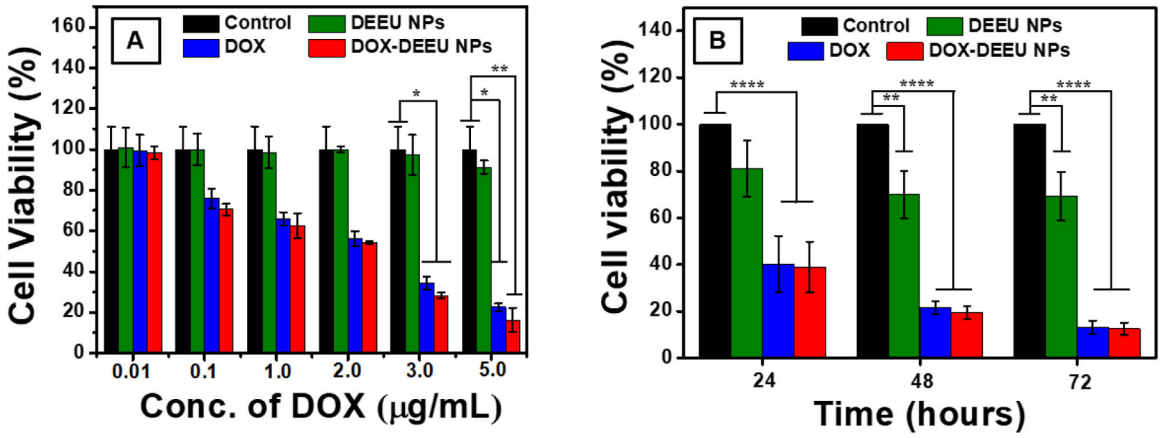

Figure 7.

Cell viability studies of HCT116 cells after treatment with pure DEEU NPs, DOX, and DOX-DEEU NPs (A); Cell proliferation studies showing quantitative estimation of the cell viability for different treatment groups (DEEU NPs, DOX, and DOX-DEEU NPs) with respect to control as a function of time (B). (*** means $p < 0.001$)

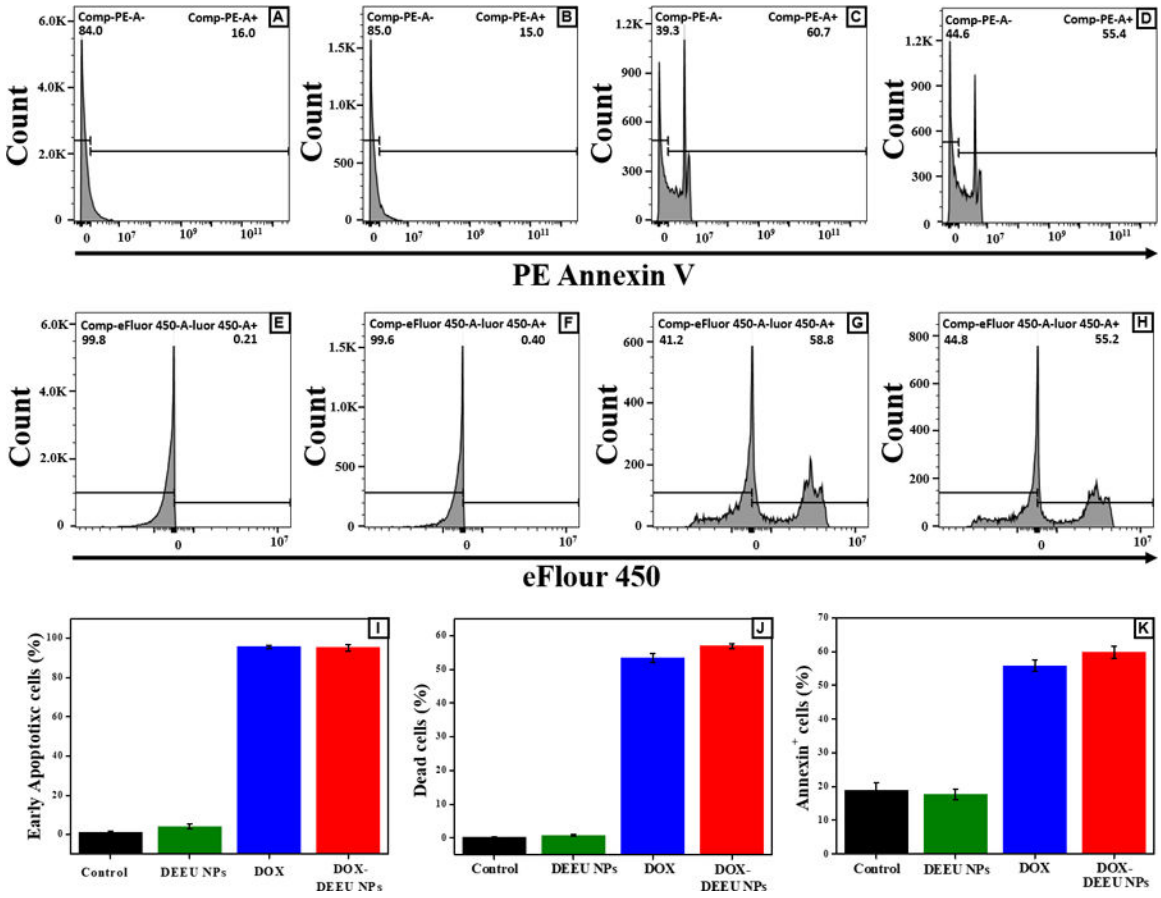

Figure 8.

Flow cytometry analysis and cell-death status of control, DEEU NPs, free DOX, and DOX-DEEU NPs (A-H); percentage cells in each phase for DEEU NPs, free DOX, and DOX-DEEU NPs (I-K).

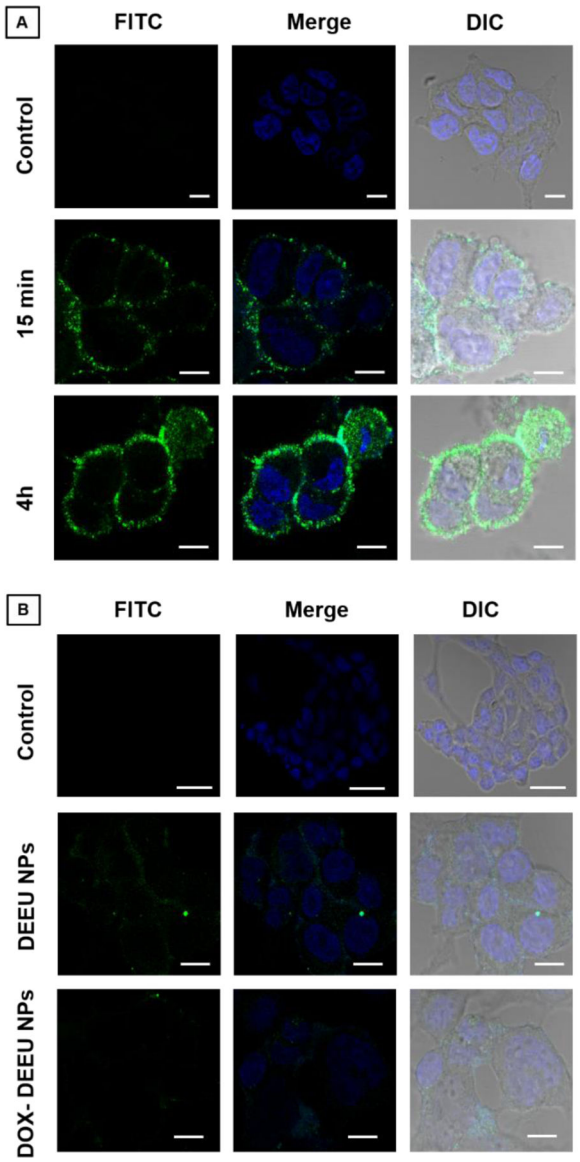

Figure 9.

Cellular uptake of FITC-tagged DOX-DEEU NPs in HCT116 cells after 15 min and 4 h (A); FITC-tagged DEEU NPs, and DOX-DEEU NPs in HEK293T cells after 4 h (B). Scale bars correspond to 100 μm.

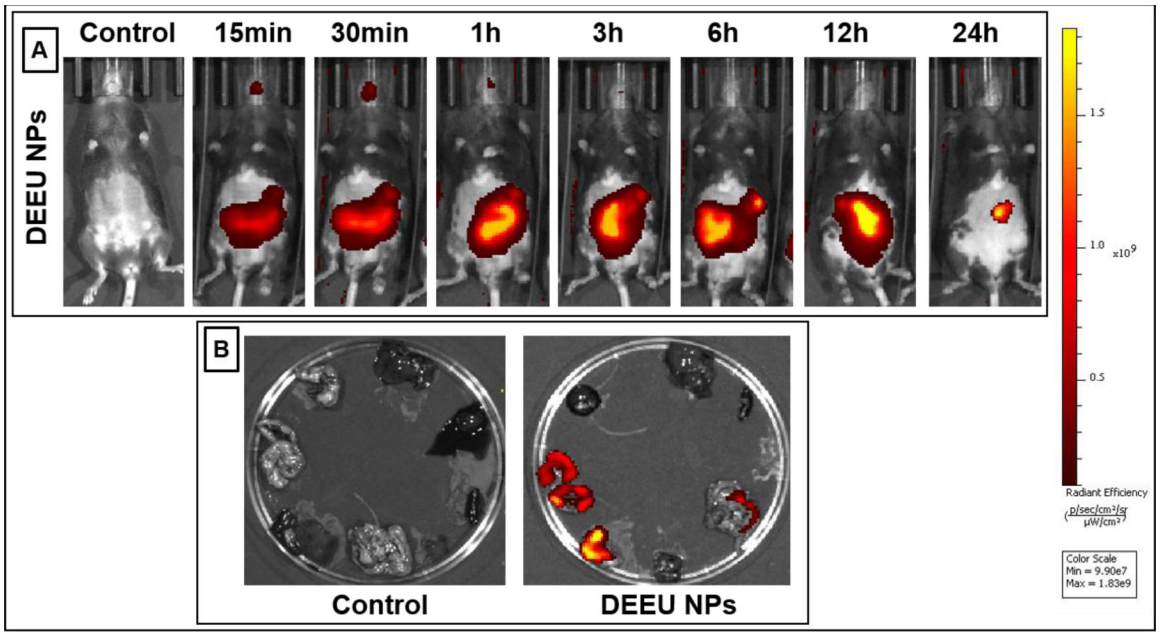

Figure 10.

Fluorescence images showing *in vivo* biodistribution of ICG tagged DEEU NPs at regular time intervals as compared to control: Epi- fluorescence images from the whole body (A). *Ex vivo* fluorescence images of DEEU NPs after 24h of oral administration: Epi-fluorescence images of internal organs from control and DEEU NPs administrated mouse (B). Experiments were performed in triplicate. The spectrum gradient bar reflects the relative fluorescent level.

Table 1.

Average hydrodynamic diameter (D_{Hyd}), average PDI, and free −SH groups estimation in various DEEU NPs samples synthesized using different ratios of TDE and TEU.

Sample code	TDE: TEU ratio	D_{Hyd} (nm) (Average)	PDI (Average)	−SH amount (μg thiol/mg DEEU NPs)
TDE	-	-	-	21
TEU	-	-	-	54
DEEU−1	1:0.25	479	0.59	2.6
DEEU −2	1:0.5	235	0.16	0.49
DEEU −3	1:0.75	419	0.44	2.0
DEEU −4	1:1	341	0.63	1.6